Wires for spring construction: full scale fatigue experimental tests

F. Ballo, M. Carboni, G. Mastinu, G. Previati

This is a post-peer-review, pre-copyedit version of an article published in Meccanica. The final authenticated version is available online at:
https://doi.org/10.1007/s11012-021-01448-7

DIPARTIMENTO DI MECCANICA ■ POLITECNICO DI MILANO
via G. La Masa, 1 ■ 20156 Milano ■ EMAIL (PEC): pecmecc@cert.polimi.it
http://www.mecc.polimi.it
Rev. 0

Noname manuscript No.
(will be inserted by the editor)

Wires for spring construction - full scale fatigue experimental tests

F. Ballo · M. Carboni · G. Mastinu · G. Previati

Received: date / Accepted: date

Abstract The paper deals with the experimental assessment of the fatigue life of wires for spring construction. Fatigue testing of full-scale wires is not a well established procedure. The aim of the paper is to demonstrate that the fatigue properties of full-scale wires for spring construction can be assessed with a level of accuracy comparable with tests performed on standard small-scale specimens. For this purpose, a new bench able to perform high frequency tests for the characterization of the wires in the high and very high cycle fatigue regions is designed, built and employed. The failure mechanism of the tested wires is described by an in-depth analysis of the fractured surfaces. By a comparison with available literature data, the difference with respect to similar tests performed on small-scale specimens is highlighted. Performing the tests on the full-scale wires allows the assessment of the effectiveness of the manufacturing process. The effect of the actual surface finishing on the fatigue life of wires can be assessed.

Keywords Four point bending · drawn steel wire · high cycle fatigue · very high cycle fatigue

Nomenclature

$2a_2$	Pitch of adjacent roughness notches along the load axis
δp_i	Uncertainty associated to each parameter p_i
Γ	Curvature of the beam
μ	Mean value
σ	Standard deviation
σ_a	Fatigue stress amplitude
σ_w	Endurance fatigue limit
σ_{max}	Stress on wire outer surface
$\sqrt{area_R}$	Equivalent defect size
a	Distance between central and lateral supports
a_1	Roughness notch depth
b	Distance between the two central supports
d	Wire diameter
E	Elastic modulus
h	Dial gauge readout
HV	Vickers Hardness
J	Moment of inertia of the beam cross section
l	Span of the arcmeter
m	Inverse slope of Wöhler's curve
$M(x)$	Bending moment on the beam
N_f	Cycles to failure
P_1	Force acting at each of the two central supports
R_a	Arithmetic mean surface roughness
R_t	Total height of the roughness profile
T_σ	Scatter index of Wöhler's curve
u_{TOT}	Total measure uncertainty
$v(x)$	Beam transversal displacement
v_1	Transversal displacement of the two central supports
x	Position along beam axis

Politecnico di Milano - Dep. of Mechanical Engineering
Via La Masa 1
E-mail: giorgio.previati@polimi.it

1 Introduction

The fatigue life of springs is a well discussed topic and several papers can be found in the literature [1–4]. High cycle fatigue (HCF) and very high cycle fatigue (VHCF) regimes are investigated. In [1], it is pointed out that failures of springs at 10^7 cycles are mostly due to surface notches, while for higher number of cycles, are due to subsurface inclusions [2]. Even if surface notches can

be mitigated by surface treatments, such as shot peening, a viable way to increase the fatigue life of springs is to improve the manufacturing process as to reduce both surface notches and internal inclusions [1, 3]. In this perspective, to increase the performances of spring steels and to have a reliable quality assessment of the manufacturing process, a rigorous verification of each step of the process should be implemented.

One fundamental step in the manufacturing of the springs is the construction of the steel wire to be shaped in the final geometry of the spring. The wire is a slender beam of circular cross section that is then plastically and permanently deformed to obtain different typologies of springs. The verification and characterization of the mechanical properties and strength of the wire is a critical point, as defects possibly present in the wire will be present in the final spring, as well. Testing the wire is not, however, a consolidated process. As surface finishing and subsurface inclusions are relevant for the fatigue life of the obtained spring, testing the wire material against fatigue, by using standardized small-scale specimens extracted from the wires, does not seem to completely address the issue [5]. Indeed, to transfer results from small-scale specimens to full-scale wires in a reliable way, low differences in material and stress state have to be present [6] for both surface and subsurface failure mechanisms. On the other hand, testing full-scale wires requires a specific equipment.

In the literature, some test benches for fatigue testing of wires are proposed. From this point of view, the fatigue properties of wires are commonly assessed by rotating bending fatigue tests [7, 8]. This seems due to two facts. First, as discussed in Section 2.1, all of the springs manufactured using wires are particularly prone to bending fatigue. Second, while a torsional fatigue load is impractical and, maybe, even impossible to apply to full-scale wires, rotating bending can be accomplished more easily. In Section 2.2, a detailed discussion of the test benches available in the literature is given. In all of the mentioned implementations, rotating bending is considered. However, none of them seems to be able to perform the test without applying also some spurious stresses to the wire. For this reason, a novel test bench will be discussed in the first part of the paper.

In the second part of the paper, the failure mechanism, observed testing full-scale wires against rotating bending fatigue by the proposed test bench, is discussed. Referring to HCF and VHCF, few experimental data are available in the literature on full-scale wires and finished springs. Particularly, in [3, 4], several finished coil springs are tested in the VHCF regime. However, the material properties and surface finishing of the tested springs are rather different from those of the wires, as surface and thermal treatments are usually performed in the final stage of the manufacturing process. A larger amount of literature data is available on spring materials tested using standardized small-scale specimens, as, for the exemplificative case of the VHCF regime, those reported in [1, 9–11]. Being the data presented in these papers related to materials, they should be properly elaborated in order to be useful for representing the behaviour of full-scale wires. In the last part of the paper, fractographic images and Murakami's model [12] for the effect of defects on fatigue strength are employed to compare the data referring to small scale specimen to the data referring of full-scale wires and to better understand the failure mechanisms involved.

The paper is organized as follows. Section 2 is devoted to the analysis of the role of bending on the failure of wire springs and to the analysis of currently available test benches for full-scale wire fatigue testing. Then, in Section 3, the conceptual design of the proposed novel test bench is described. The experimental assessment of the effectiveness of the designed bench is discussed in Section 3.2. Specifically, two prototypes of the bench have been manufactured and both were used to derive the Wöhler's curve of 39NiCrMo3 ground steel bars. Results are compared to each other, in order to check the accuracy and repeatability of the results themselves, and to relevant literature data, in order to validate the bench rigorously and in absolute terms. Finally, in Section 4, the fatigue properties of high strength wires, employed for spring manufacturing, are experimentally investigated in the HCF and VHCF regimes. After a careful analysis of the failure mechanism, the validation of the experimental set-up and of the proposed bench is fully achieved by the comparison to and discussion of literature data obtained from tests on small-scale specimens made of the same spring steel grade and by the application of Murakami's model for the effect of surface roughness on fatigue strength [12].

2 Full-scale fatigue testing of wires for spring construction

In this section, some preliminary information about wire testing are provided. Firstly, the relevance of bending load in spring failures is deeply analyzed. Then, the currently available test benches for wire testing are discussed.

2.1 Bending as the important stress factor for wire springs

Fig. 1 shows some examples of common springs with their loading pattern: all of them have an active region with a circular cross section, most of them are manufactured exploiting wires. Indeed, bare torsion springs (torsion bars, Fig. 1 b) are not typically manufactured using wires because their extremities must be shaped with bulk parts for the torque to be applied effectively. Excluding torsion springs, it can be stated that spring wires are typically subjected either to bending or to a combination of torsion and bending. Moreover, despite torsion is reputed to be the main dangerous stress in coil springs such as the ones shown in Fig. 1 c, experimental evidence states that bending is a non-negligible failure mode, as well. From this point of view, [13] reports that, often, coil springs, which should fail due to torsion, do fail due to bending at the ground ends. The same conclusion is drawn in [3, 4], where shot peened coil springs proved to fail at the coil ends due to excessive bending stress. Finally, in [14], the authors report that a compression coil spring, fitted on a heavy vehicle, fractured at the transition position from the bearing coil to the first active coil in service due to an excessive bending stress.

In this paper, the attention is focused on bending fatigue testing rather than on torsion or on mixed bending-torsion testing because of the just mentioned observations. Nevertheless, another reason for focusing on bending is that clamping wires for torsional fatigue testing is still extremely tricky, since the requirement is to avoid applying concentrated forces or moments that may influence experimental results. This issue, at the current state of the art, is crucial and unsolved for the concept design of an effective torsional fatigue bench for full-scale wires. Obviously, an in-depth study could overcome this issue, but this is beyond the aim of the present research and, being bending a relevant structural issue for wire springs, rotating bending is here considered.

Finally, it is well known that the presence of defects has an important effect on the fatigue strength of materials [12]. In Fig. 2, an exemplificative manufacturing defect of a drawn wire is shown. As one may understand, defects located near the external surface of the wire, as the one of Fig. 2, are the most dangerous for the safety of the spring. Indeed, both bending and torsional stresses applied to the wire reach their maximum on the surface of the wire. This fact assures that considering only bending actions is still a relevant approach to keep into account the influence of surface and sub-surface defects on the fatigue strength of full-scale wires.

2.2 Rotating bending as the only viable way to assess fatigue properties of wires

Rotating bending seems to be the easiest way to assess fatigue properties of wires, even if testing is not straightforward. In [7, 8], a Haigh – Robertson rotating–beam machine, shown in Fig. 3 ([16]), is used for applying rotating bending fatigue to wires. First, a constant amplitude bending moment was applied to a long piece of a wire by suitably tilting the two supports located at its extremities. Second, the wire was put in rotation, about its axis, by a motor. Due to the high clamping moments at the supports, most of the failures were localized there. To avoid such a problem, the section of the tested wires was reduced, along the free span between supports, by proper machining. This, in our opinion, makes the application meaningless with respect to the previously stated goals. Indeed, the fatigue strength of the full-scale wire depends strongly on its surface conditions. The machining process applied to the free span of the wire involves deep modifications of the surface finishing of that portion of the wire, thus making the obtained results not representative of the actual manufacturing process of the full-scale wire. It is clear that, since the focus is on the characterisation of the full-scale component, the tested specimens cannot undergo any mechanical or thermal modification after the actual manufacturing process.

Fig. 4 shows a four point rotating bending machine by Nakamura [17]. This machine considered three supports. The fourth support was a bending point obtained by the connection of the wire to the motor. In case of wires with large diameter this solution involves a significant transversal force on the motor shaft, which reduces its reliability. The designer is forced to select a large-size motor. Moreover, with the three supports scheme, the relative position between the centre of the hinge of the motor support and the centre of the clamping jaw on the wire has to be accurately controlled. In fact, if these two points are not well aligned, a spurious concentrated moment arises at the connection between the motor and the wire. A vinyl chloride bushing was interposed between each bearing and the wire in order to reduce stress concentration, but, nevertheless, failures occurred often in correspondence of supports.

Commercial four points rotating bending machines for wires are available [18, 19], as well. As shown in Fig. 5, four rotatable bearings are the supports. The two central supports can move along the vertical direction to apply the load to the wire. An electric motor

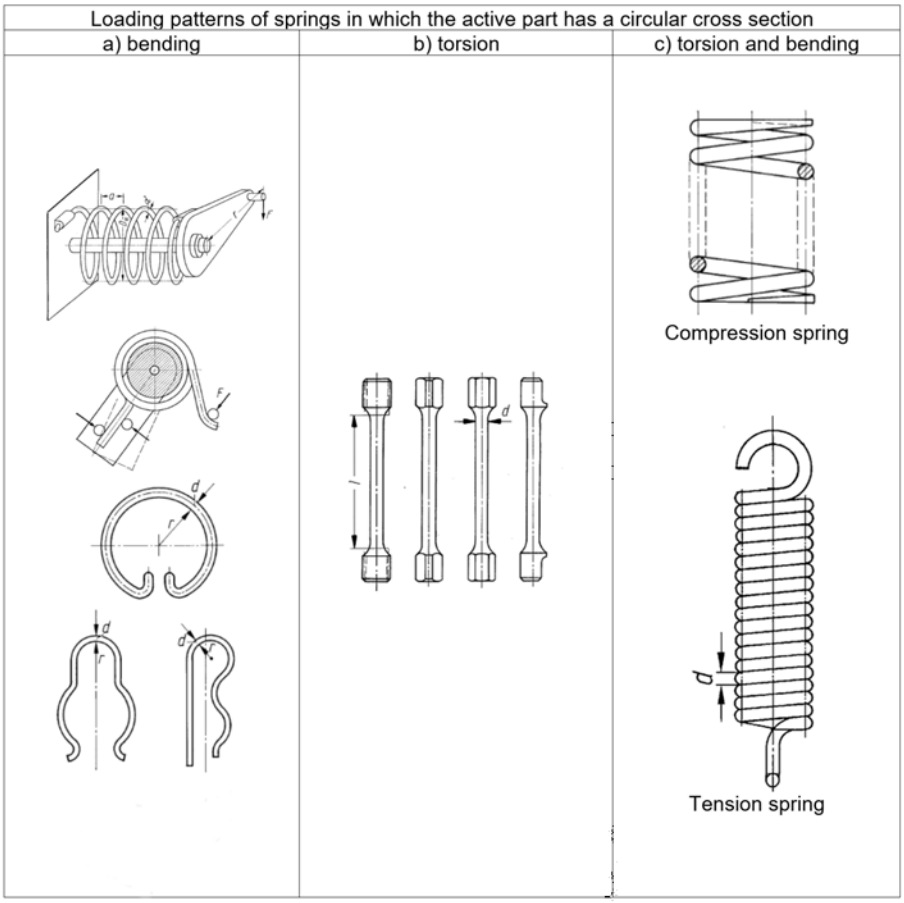

Fig. 1 Springs whose active part is a slender beam of circular cross section: a) springs subjected to bending stresses only; b) springs subjected to torsional stresses only; c) springs subjected to torsional and bending stresses. Just a) and c) springs are commonly manufactured employing wires. Adapted from [15].

Fig. 2 An exemplificative manufacturing defect on the surface of a wire. Courtesy of F.A.R. S.p.A.

is mounted on a pivot in such a way to follow the wire displacement during the load application. The remaining misalignment between the motor axis and the wire is compensated by an elastic torsional joint. Such kind

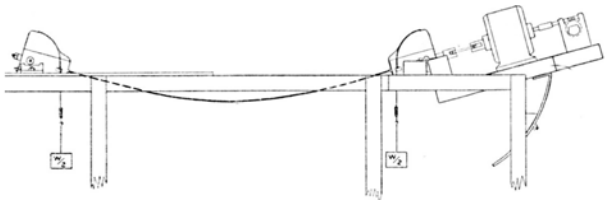

Fig. 3 Haigh-Robertson's testing machine for wires, adapted from [16].

of joint allows to transmit the motor torque to the wire by allowing a relative rotation between the motor axis and the wire axis. Curved-shaped bushings are used at the interface between wire and supports to reduce stress concentrations.

This type of architecture, although more effective than the original Nakamura's testing machine of Fig. 4, still provides some spurious bending load at the connection between the wire and the motor. Such bending load is due to the (small) bending stiffness of the torsional joint, which can provide significant deviations from the pure four-point bending loading scheme, especially in

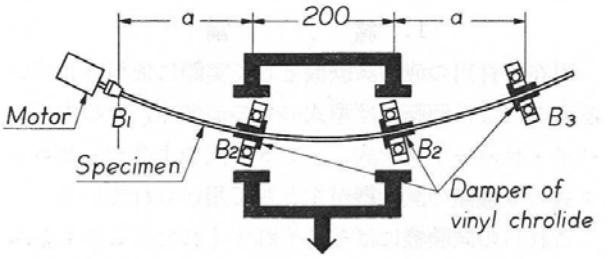

Fig. 4 Nakamura's testing machine for wires [17].

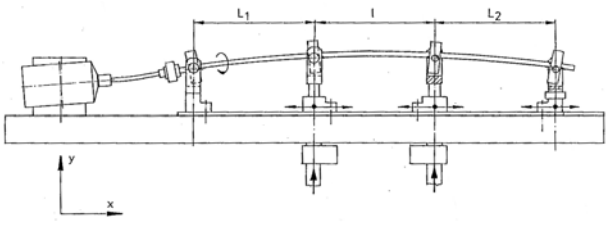

Fig. 5 IABG's testing machine for wires, adapted from [18].

case small wires are tested, whose bending stiffness is comparable to the one of the joint.

From the above analysis, it can be concluded that none of the known machines for assessing the fatigue properties of wires is fully suitable for:

- applying a pure four-point rotating bending static scheme
- reducing the interaction between the wire surface and the supports
- allowing the test of a large variety of wire diameters with the same architecture.

In the paper, an enhanced bench, able to overcome the described shortcomings, is proposed.

3 Novel test bench for rotating bending fatigue of wires

The preliminary design of the test bench has been presented by the authors in [20]. Here, the main design principles are briefly summarized along with the description of the most relevant features implemented to overcome the above mentioned shortcomings of currently available test benches.

Fig. 6 shows the static scheme of the machine, which is able to locate and test wires with diameters ranging from 6 to 20 mm.

The first difference with respect to the test benches presented in Section 2 is the arrangements of the elements of the test bench in the horizontal plane. In this way, the gravity does not affect the positioning of the electric motor that can then be accurately aligned to the direction of the axis of the wire coming out from the

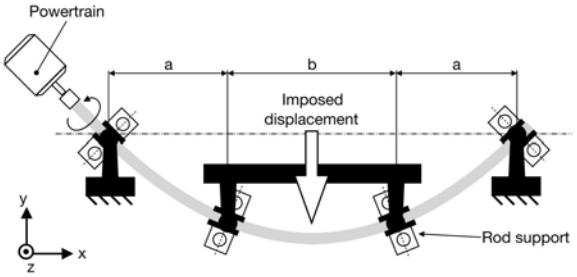

Fig. 6 Static scheme of the four point rotating bending test bench.

first support. The wire is bent by displacing the two central supports along a transversal direction with respect to the wire undeformed axis. To avoid any misalignment, the two central supports are rigidly connected to each-other. The wire is set in rotation through a two-poles asynchronous three-phase electric motor having a nominal power of 1.5 kW and a maximum rotational speed of 3000 rpm.

The motor is connected to the wire by a special elastic joint transmitting the required torque. Extreme care has been put in avoiding any spurious bending load due to the motor positioning. During the load phase, while the displacement is imposed, the motor is free to move on the test bench plane by a pneumatic friction-less support system. In this way, the position and orientation of the motor is given by the deformation of the wire, i.e. the wire is free to deform without any additional constraint. As the desired deformation level is reached, the support system is locked in position.

In Fig. 7, the reaction forces and the bending moment acting on the wire when subjected to a four point bending loading scheme are reported. The region between the two loads P_1 represents the zone of the wire where a constant bending moment is present. Theoretically, any point of this region has the same probability of failure. The actual failure will occur in correspondence of the largest inclusions or defects (when present) on either the surface or the sub-surface region of the wire. It has to be emphasized that at the edges of this region, i.e. where the reaction loads P_1 are applied, the bending moment reaches the maximum value. It means that, to avoid localized failures in the correspondences of the supports, they must be suitably designed in order to avoid any stress concentration. Such a feature was obtained by means of specifically designed bushings, made of polyethylene terephthalate (PET) polymeric material, whose internal surface, i.e. the surface directly in contact with the tested wire, has a curved profile defined to maintain a uniform bending stress distribution in the contact area between the wire and the bushing [20]. The effectiveness of the bushing with a curved

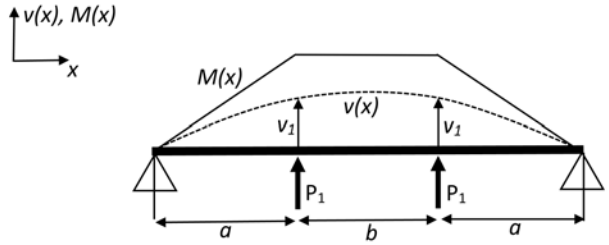

Fig. 7 Four point rotating bending test. Bending moment diagram and beam transversal deflection.

profile appears evident in Fig. 8, which shows the stress acting along the axis of the wire near one of the central supports: the use of curved bushings (dashed lines) allows to maintain a more uniform and constant stress in the central section of the wire both for small (Fig. 8 left) and large (Fig. 8 right) wires. Additionally, in the diagrams of Fig. 8, the contact areas between the bushing and the wire are marked with circles: the double contact point state associated to the cylindrical profile introduces a significant perturbation in the stress due to the bending moment applied to the wire as shown in Fig. 8 for wires of 6 mm and 20 mm of diameter. In such a situation, spurious bending stresses are present and the fracture is localized at the inner contact point. The dotted lines show the stress due to bending moment when specially designed hyperbolic surfaces are employed. The stress copies the ideal distribution due to four point bending and the fracture happens randomly between the two central supports depending of the defect distribution. The shown stress distributions were obtained by a finite element model of the system [20].

During the test, the wire is rotated in order to apply a sinusoidal fatigue load. To reduce the testing time, a high rotational velocity (up to 3000 rpm) is required. To avoid vibrations of the wire, its first bending eigenfrequency should be higher than the rotational frequency. Both analytical and numerical analyses have been conducted to evaluate the dynamic behaviour of the wire - the reader could refer to [20] for a detailed description. Results confirmed that the lowest expected natural frequency of the wire is greater than 50 Hz (the maximum frequency of the two-poles motor employed in the bench).

Fig. 9 shows the assembled test bench and a detail of a fatigue-failed wire.

3.1 Measurement of the stress on the wire

The bending stress applied to the wire is measured indirectly by measuring the imposed curvature. By considering the notations of Fig. 7, the curvature of the wire can be computed as [21]:

$$\frac{M(x)}{EJ} = \frac{\dfrac{d^2v}{dx^2}}{\left[1+\left(\dfrac{dv}{dx}\right)^2\right]^{\frac{3}{2}}} = \Gamma(x) \tag{1}$$

where $M(x)$ is the applied bending moment, E the elastic modulus of the material, J the (constant) moment of inertia of the section and $v(x)$ is the transversal displacement of the wire, with first derivative $\dfrac{dv}{dx}$ and second derivative $\dfrac{d^2v}{dx^2}$. Γ is the curvature of the beam, which is proportional to bending moment (and therefore to the bending stress) acting on the wire.

Eq. 1 refers to the curvature-bending moment equation of the beam for the general case of large displacements. Such an equation could be simplified by considering $\dfrac{dv}{dx} \simeq 0$ if the transversal displacement is less than 10% of the span of the beam. In the present case, if high values of stress are reached, this condition is not met and the formulation for large displacements has to be considered. Eq. 1 is a differential equation of the second order, its solution can be found by numerical integration along the beam axis. The resulting solution is a function of:

- lengths of the sections of the wire (parameters a and b of Fig. 7)
- imposed displacement v_1 of the two central supports
- material and cross section parameters (E and J)

Given the value of the wire curvature Γ and under the reasonable assumption of large radius of curvature of the beam with respect to the beam diameter, the maximum stress, acting on the surface of the beam, reads

$$\sigma_{max} = E\Gamma\frac{d}{2} \tag{2}$$

where E is the elastic modulus of the (homogeneous, linear elastic) material the wire is realised from and d the diameter of the wire. Based on this approach, a special arc-meter able to measure the curvature Γ of the loaded wire has been designed and realized. The instrument is shown in Fig. 10 and is realized by a dial gauge mounted on a specifically designed steel structure. The dial gauge has a measuring range of $0-10$ mm, a resolution of 0.01 mm and is mounted on the rectangular steel element shown in Fig. 10 (left). Two knife edges made of tempered steel are mounted on the two lateral surfaces of the rectangular element, at a distance of 140 ± 0.05 mm. The surfaces of the rectangular element and of the two knife edges are precisely ground to

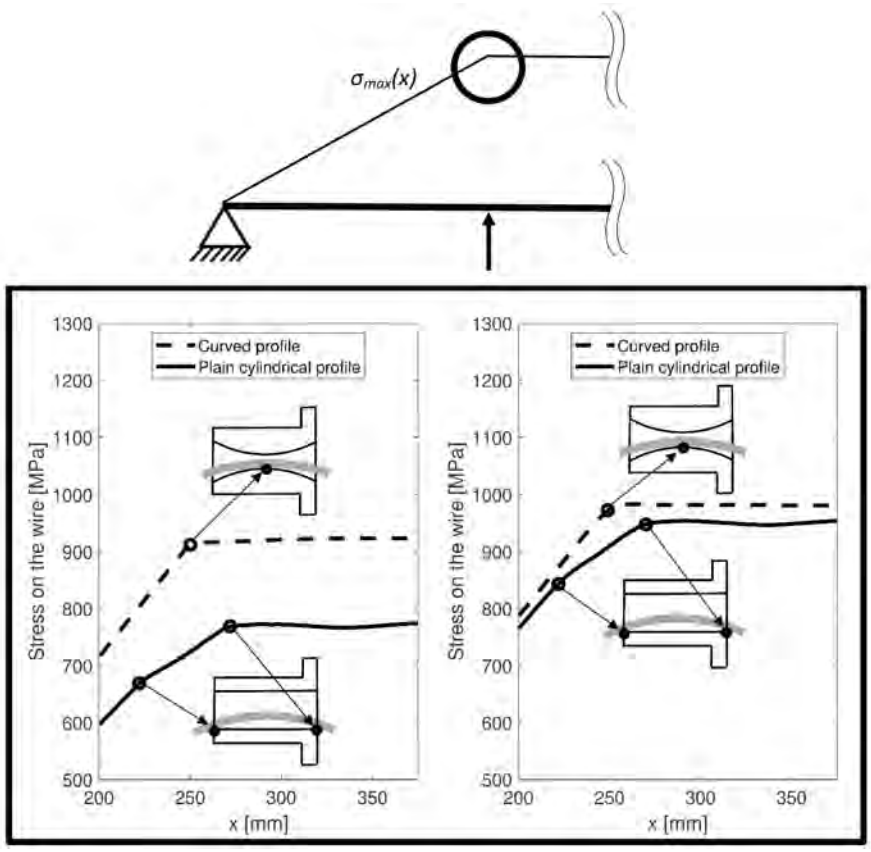

Fig. 8 Stress acting along a portion of the axis of the wire near one of the central bushings. Left: 6 mm wire and imposed transversal displacement of 84.3 mm. Right: 20 mm wire and imposed transversal displacement of 25.3 mm.

ensure tight tolerances. Finally, the entire assembly is screwed on a L-shaped support to be positioned at the height of the wire axis as shown in Fig. 10 (right). From the measure of the curvature of the wire, the (constant) stress acting along its central section can be estimated.

Being the bending moment constant and considering a reference frame with origin in point A in Fig. 10 (left), the curvature of the beam surface can be described by the equation of a circumference:

$$x^2 + y^2 - l \cdot x + \frac{(l+2h)\cdot(l-2h)}{4h} \cdot y = 0 \tag{3}$$

the radius of the circumference reads

$$r = \sqrt{\left(\frac{l}{2}\right)^2 + \left(\frac{l^2 - 4h^2}{8h}\right)^2} \tag{4}$$

and the curvature of the beam (i.e. the wire) axis reads

$$\Gamma = \frac{1}{r - \dfrac{d}{2}} \tag{5}$$

Finally, substituting eqs. 4 and 5 into eq. 2, the maximum stress in the wire can be related to the quantity h measured by the gauge (Fig. 10 left) as:

$$\sigma_{max} = E \cdot \Gamma \cdot \frac{d}{2} = E \cdot \frac{4hd}{4h^2 + l^2 - 4hd} \tag{6}$$

Eq. 6 shows that the stress measured on the wire external surface depends on the elastic modulus of the material E, on the wire diameter d, on the span of the arcmeter l and on the dial gauge reading h. The accuracy of the stress estimation depends therefore on the dimensional tolerances of both the wire and the arcmeter, on the accuracy of the dial gauge and on the uncertainty in the measure of the elastic modulus of the wire. From a mathematical point of view, assuming the parameters p_i to be independent and normally-distributed, the uncertainty in the stress estimation can be expressed as

$$u_{TOT} = \sqrt{\sum_i \left(\frac{\partial \sigma_{max}}{\partial p_i} \cdot \delta p_i\right)^2} \tag{7}$$

where δp_i is the uncertainty associated to each parameter. Considering the numerical values reported in Table 1, the overall estimated 95% uncertainty on the stress measure is limited within ±6% of the rated value.

Table 1 Numerical values of the parameters and 95% uncertainties.

Parameter description	Symbol	Nominal value	95% Uncertainty
Elastic modulus	E	206000 MPa	$\pm$10300 MPa
Wire diameter	d	d	$\pm$0.05 mm
Distance between the knives	l	140 mm	$\pm$0.05 mm
Dial gauge measure	h	h	$\pm$0.02 mm

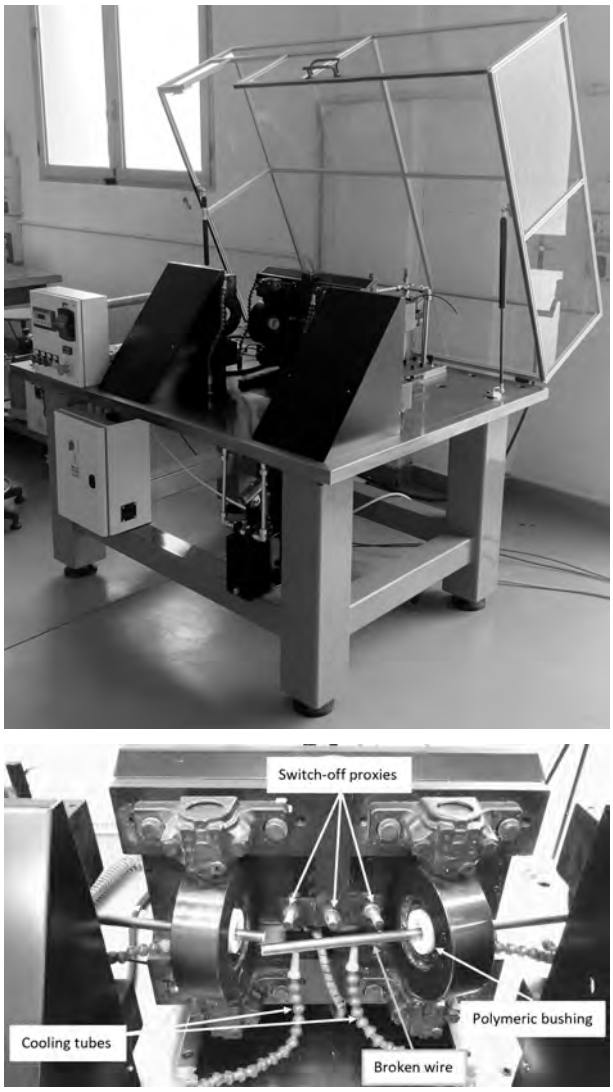

Fig. 9 Top: View of the assembled test bench with the protective cover. Bottom: detail of a fatigue-failed specimen.

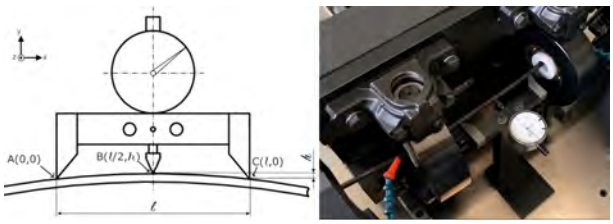

Fig. 10 Left: drawing of the arc-meter specifically designed for estimating the stress applied to the wire. Right: real arc-meter employed during an experimental test.

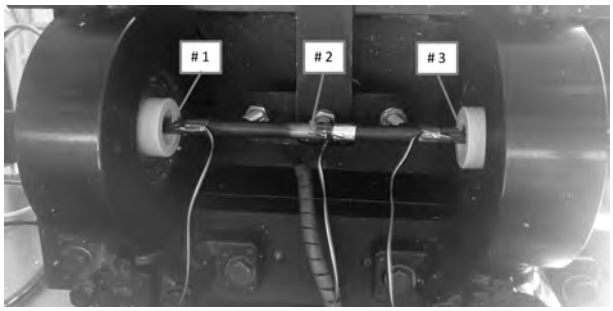

Fig. 11 Experimental setup and detail of the location of strain gauges on the sensorised wire.

3.2 Static validation of the bench

Preliminary static experimental tests have been performed to evaluate the accuracy of the model described in Section 3.1. Two steel wires with different diameters, namely 6.1 mm and 11 mm, have been sensorised with strain gauges to measure the stress on the wire surface. Three uniaxial 120 Ohm resistive strain gauges with a measuring grid of 1.5 mm have been placed on the external surface of each tested wire. The strain gauges are located at different axial positions along the wire, all the sensors are placed in the central section of the wire. The strain gauges locations are numbered from 1 to 3, being location 1 the closest to the motor. The experimental setup is shown in Fig. 11.

The signals of the three strain gauges are acquired by a Vishay® P3 strain recorder. During the test, the wire is loaded up to the desired stress level and, once such a desired stress level is reached, it is read by means of the arcmeter and by the strain gauges.

Experimental results are summarised in Table 2 for two different wire diameters at two different levels of imposed stress. The comparison between measured and estimated stress shows a maximum difference of 4.8%. As expected, the error tends to increase by increasing the diameter of the wire, having the thicker wire a higher bending stiffness. Additionally, the measured stress shows a small variability along the axis of the wire, with a maximum recorded variation of 6% for the 6.1 mm wire at low stress level. The small variability of the measured stress along the wire axis confirms the effectiveness of the bench in applying a pure bending loading scheme in the central section of the wire.

Table 2 Measured and estimated stress levels acting on the instrumented wires. The three values of measured stress refer to strain gauge location 1, 2 and 3 (see Fig. 11 for details).

Wire Diameter [mm]	Dial gauge reading [mm]	Estimated stress [MPa]	Measured stress [MPa]	Max. difference [%]
6.1	1.95	501	483, 486, 518	3.6
	3.89	999	978, 995, 1014	2.1
11	1.08	501	507, 525, 519	4.8
	2.16	1003	1029, 1042, 1041	3.9

3.3 Dynamic validation of the test bench

Two identical prototypes of the test bench have been manufactured, assembled and validated. In order to test the effectiveness of the realised test benches, dynamic tests were carried out to derive the fatigue properties of a set of commercial precise ground bars made of 39NiCrMo3 tempered steel, a material extensively analysed in the scientific literature (see for instance [10, 22, 23]). The chemical composition of the tested material, experimentally derived using a Bruker Q4 Tasman spectrometer model 130, is reported in Table 3 and results to be compliant to the nominal values specified in relevant standards [24]. The precise ground bars employed for the validation had a diameter of 8 mm, a total length of 1m and a surface roughness $R_a = 0.8\mu m$.

A set of 18 specimens has been tested on each of the two test benches to derive the Wöhler's curve of the component. Three different stress amplitudes have been tested, namely 650 MPa, 550 MPa, 450 MPa. At each stress level, six different replicas have been tested. The total number of specimens and the number of replicas for each stress level have been selected with reference to ASTM-E739 standard [25], which states that, to have reliable data, a minimum number of 12 specimens and a minimum replication percentage of 75% are required. In these tests, the total number of specimens is 18, with a replication percentage of 83%. Being the scope of such tests the dynamic validation of the benches and not the material characterisation, all the samples were tested in the finite life fatigue regime and no investigation on the fatigue limit was conducted.

All the tests have been performed at a rotational frequency of 50 Hz; the obtained Wöhler's curves are reported in Fig. 12 together with the 95% confidence band of the mean. As one may notice from the picture, the confidence bands of the two benches overlap, stating that the obtained fatigue data are statistically equivalent and, as a consequence, that the design and manufacturing process of the test bench is robust, reproducible and reliable.

In Fig. 12, the Wöhler's curves for the same material adapted from [10] are reported, as well. The reference

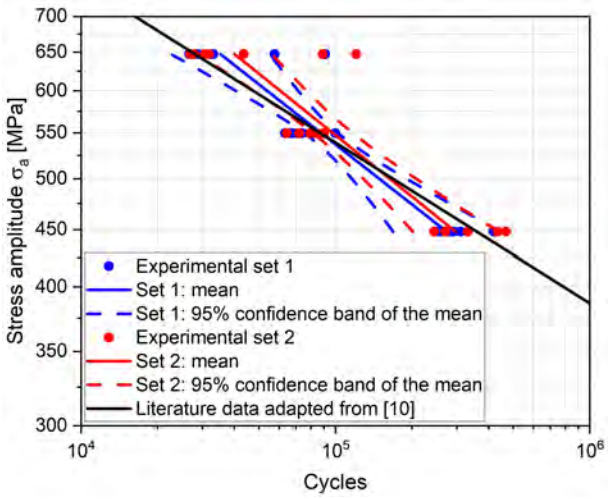

Fig. 12 Comparison of the Wöhler's curves obtained for the two sets of 39NiCrMo3 ground steel bars tested on the two benches and literature data adapted from [10].

data [10] refer to a fully reversed tension/compression fatigue test on standard specimens. For a direct comparison with the experimental data obtained in this paper, the reference data have been multiplied by 1.3 to account for the different fatigue resistance between tension/compression and bending. Additionally, a further multiplication by 0.85 is added, which accounts for the surface finishing of the bars (roughness $R_a \simeq 0.8\mu m$ and $R_t \simeq 4\mu m$) [15]. From the comparison of Fig. 12, it emerges that the mean of the two Wöhler's curves obtained for the precise ground bars, is close to the data adapted from the literature [10], confirming the effectiveness of the test benches in deriving prompt and accurate fatigue data.

4 Preliminary fatigue testing of spring wires in the high-cycle and very high-cycle fatigue regimes

A set of wires for springs was tested for a preliminary evaluation about the application of the developed bench to real full-scale components in the HCF and VHCF regimes, the latter meaning, here, up to 10^8 fatigue cycles. The considered wires were made of EN10270-2 FD

Table 3 Chemical composition [wt%] of the tested 39NiCrMo3 steel.

C	Mn	Si	Cr	Ni	Mo	P	S
0.436	0.763	0.197	0.859	0.788	0.246	0.012	0.027

SiCr steel [26], corresponding to a 54SiCr6 low alloy grade, whose chemical composition is reported in Table 4 in terms of mean values (μ) $\pm$ standard deviations (σ). In particular, as for the case of the 39NiCrMo3 steel grade described in Section 3.2, the experimental derivation of the shown chemical composition was carried out by the aforementioned Bruker spectrometer considering eight different small chunks directly cut from the tested wires.

The tested wires were manufactured as follows: i) surface preparation through both chemical and mechanical treatments; ii) cold-drawing; iii) thermal treatment by tempering and oil hardening in order to achieve the required mechanical properties, which are shown in Table 5 in terms of mean values (μ) $\pm$ standard deviations (σ). It is worth adding the reported mechanical properties were experimentally derived by tensile testing, according to [27], four dog-bone specimens extracted by the tested wires, while the Vickers hardness was indirectly derived, using the conversion rules suggested in [28], from Rockwell C hardness measurements carried out according to [29].

Fatigue tests were carried out on wires whose diameter was equal to 11.5 mm and according to the test plan shown in Table 6, where test results are reported, as well. In particular, the total number of tested specimens was 14 and it is worth noting that, for considering a given result as a successful one, failure had to occur between the central supports. Of all the tested wires, just one showed a failure located outside the central section, although very close to one of the supports of the central section. This fact confirms that the designed polymeric bushings are able to lower effectively the stress concentration at the interface surfaces.

A first qualitative evaluation of the obtained fatigue data, and consequently of the performance of the proposed bench, was carried out comparing them to those of a very similar, see Table 4 and Table 5, "Clean 54SiCr6" steel grade studied by Zhang et al. in [9]. It is worth remarking these comparative data were derived from standardized mirror-polished small-scale specimens characterized by a 3 mm diameter at the tested section. Despite the just mentioned relevant differences of the features of the adopted specimens, both datasets show a qualitatively similar underlying behaviour (Fig. 13). In particular:

– the fatigue durability is the same at high load levels (900 MPa)

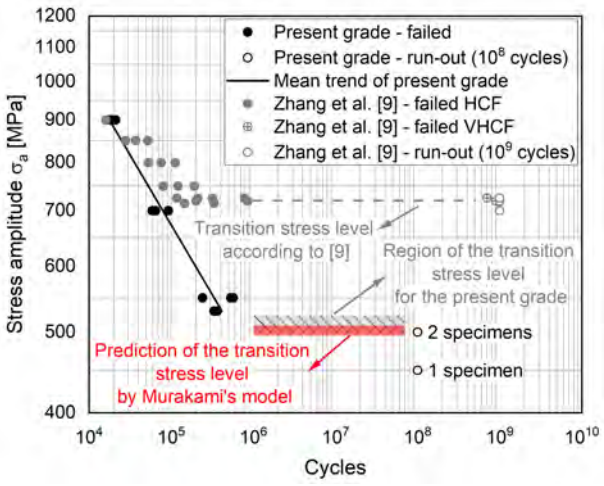

Fig. 13 Wöhler's curves obtained for the considered spring wires.

– an abrupt (and clear) transition, between HCF and VHCF regimes and characterized by a horizontal, or nearly horizontal, transition stress level, is evident. Such a stress level is declared to be equal to 720 MPa by Zhang et al. for their grade [9] and is just indicated, in Fig. 13, by a dashed grey horizontal line. On the other hand, for the present grade manufactured in terms of wires, the transition stress level lies between the lowest load level of the failed specimens and the highest of the run-out ones (shaded grey region in Fig. 13), because not enough data are available for a more accurate estimation
– the end of the HCF regime seems to occur at the stress level providing a fatigue durability equal to about 10^6 cycles. In Table 7, the inverse slope m and the fatigue scatter index $T_{\sigma,10^6}$ (10%-90%) of the Wöhler's curves of the two sets of data of Fig. 13 are reported
– Zhang et al., in [9], show the same kind of fatigue data for other three spring steels and their fatigue behaviours result to be significantly different, also in qualitative terms, with respect of the two datasets shown in Fig. 13

On the other hand, some important discrepancies, between the two datasets, have to be highlighted, as well. First, interrupting the fatigue tests on the present grade at 10^8 cycles, it was not possible to gather failures based on typical VHCF damage phenomena. This can be explained by observing again Fig. 13 and noting that the VHCF failures by Zhang et al. appear after about

Table 4 Chemical composition [wt%] of the considered 54SiCr6 steel grade and of a reference one from the literature.

	C	Si	Mn	Cr	P max.	S max.
Present grade	0.58 ± 0.02	1.48 ± 0.02	0.69 ± 0.01	0.67 ± 0.01	0.012	0.01
Zhang et al. [9]	0.56	1.45	0.70	0.65	0.012	0.01

Table 5 Mechanical properties and Vickers hardness of the considered steel grade and of the reference one.

	Elastic modulus $[GPa]$	Ultimate tensile strength [MPa]	HV
Present grade	209 ± 1	1779 ± 7	485 ± 9.5
Zhang et al. [9]	209.6	1743	500

Table 6 Fatigue testing plan and results.

Sample	Rotational speed [rpm]	Stress amplitude σ_a [MPa]	N_f	Fracture location
01	3000	900	18700	central section
02	3000	900	21100	central section
03	3000	900	17770	central section
04	3000	700	92700	central section
05	3000	700	58800	central section
06	3000	700	64850	central section
07	3000	550	534700	central section
08	3000	550	571850	central section
09	3000	550	241700	central section
10	3000	530	363000	central section
11	3000	530	333230	outside
12	3000	500	$> 10^8$	–
13	3000	500	$> 10^8$	–
14	3000	450	$> 10^8$	–

Table 7 Inverse slope and scatter index (10%-90%) of the HCF data of Fig. 13.

Dataset	Inverse slope m	Scatter index $T_{\sigma,10^6}$
Present grade	6.26	1.17
Zhang et al. [9]	12.35	1.60

10^9 fatigue cycles, an amount not reached during the present tests. Nevertheless, the aim of the present paper is not the VHCF characterization of the present grade, but the design and validation of the test bench and, in these terms, the run-outs at 10^8 fatigue cycles, obtained by the proposed bench, are fully compliant with Zhang et al.'s data. The second evident discrepancy between the two datasets consists in the relevant difference between the transition stress levels and, generally, in the slopes of the corresponding Wöhler's curves. Intuitively, the rationale for a significantly lower transition stress level of wires could be found in the different condition, with respect to Zhang et al.'s specimens, in terms of surface finish, dimensional effect of the tested sections and of the defect "clean" condition of small-scale specimens which is not met by the tested full-scale wires. The remaining part of this Section is devoted to better understand and quantify the reasons of such a lower transition stress level of wires and to check if the results provided by the proposed bench are reasonable and physically meaningful, i.e. if the bench can be definitely validated.

Fig. 14 shows some illustrative fractographic images of sample #02, tested at a high load level (900 MPa), while Fig. 15 some others of sample #07, tested at a relatively low load level (550 MPa). The shown fracture surfaces were acquired by means of a WILD M3Z high-definition optical stereo microscope after cutting a 20 mm long portion of the failed specimens from the fracture surface themselves. A 4% oil/water mixture coolant was used during the cutting operation to prevent any heating of the fracture surface; additionally, a plastic-paraffin film protection was applied to the fracture surface to avoid any contamination.

By observing the general view of the fracture surface shown in Fig. 14 (top left), the typical features of a high load rotating bending fatigue failure can be clearly noted: a relatively large final failure zone ("F" in the figure), a primary crack, originating the final failure, characterized by evident beach marks ("B") denoting fatigue crack propagation, the presence, in the initiation region of the primary crack, of ratchet marks ("R") typically denoting the coalescence of multiple initiation sites located in adjacent, but slightly translated along the axial direction of the wire, planes and the initiation of secondary cracks ("S") outside the primary crack. It is worth noting that the observation of multi-

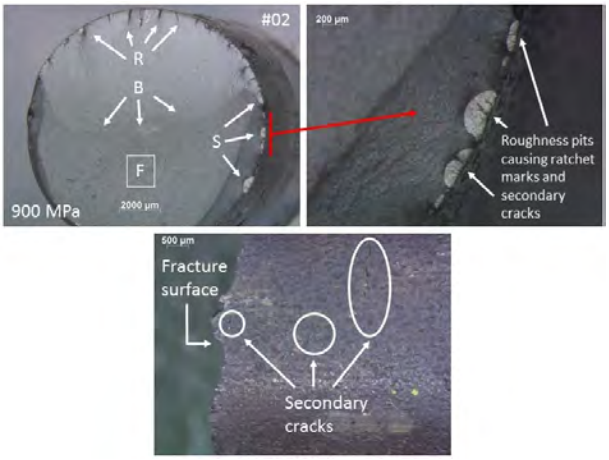

Fig. 14 Fractographic images of sample #02, tested at 900 MPa. F = final failure zone; B = beach marks; R = ratchet marks; S = secondary cracks.

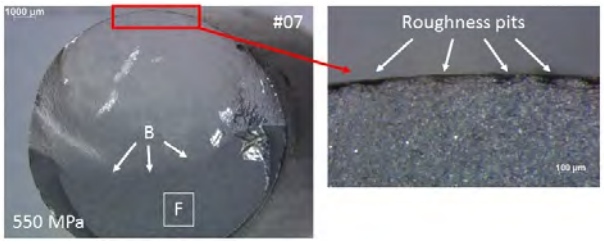

Fig. 15 Fractographic images of sample #07, tested at 550 MPa. F = final failure zone; B = beach marks.

ple crack initiation sites inside (ratchet marks) and outside the primary crack indicates, for the case at hand, that fatigue damage was not triggered by relevant local discontinuities or flaws, but by a general and uniform favourable condition of the whole surface of the specimen. In particular, such a favourable condition was found to be strictly related to the inherent surface finish (roughness) of the wires. This conclusion is supported by both Fig. 14 (top right), where it is highlighted that each secondary crack initiated at a roughness pit, and Fig. 14 (bottom), where other secondary cracks, located at different axial sections of the wire and characterized by peculiar paths following the roughness local pattern, are shown. The latter figure also allows noticing the typical surface finish condition and roughness morphology of the considered wires. Roughness measurements were, then, carried out, by a Mahr MarSurf PS1 rugosimeter, on four different wires and allowed estimating $R_a \simeq 1.8\mu m$ and $R_t \simeq 9\mu m$, i.e. values significantly higher than those of Zhang et al.'s mirror-polished specimens.

To provide a further example, the same conclusions could be drawn by observing the general view of the fracture surface shown in Fig. 15 (left), where the typical features of a relatively low load rotating bending fatigue failure can be noted: in this case, as expected, neither ratchet marks, nor secondary cracks are present and the final size of the primary crack gets bigger before the final failure. Nevertheless, the initiation site of the primary, and only, fatigue crack is still characterized by the presence of evident roughness pits (Fig. 15 (right)).

Since surface finish seems to play a relevant role on the fatigue failure of the considered wires, the last step of the investigation consisted in the estimation of the transition stress level, and the comparison to the value provided by the proposed bench, using the model by Murakami for the effect of surface roughness on fatigue strength [12]. Such model allows estimating the endurance limit of a material, i.e. the transition stress level for the case at hand, by the following expression (already adapted for the special case of rotating bending):

$$\sigma_w = \frac{1.43\,(HV + 120)}{(\sqrt{area}_R)^{\frac{1}{6}}} \tag{8}$$

where HV is the Vickers Hardness of the material and $\sqrt{area}_R$ is an equivalent defect size, for surface roughness, accounting for both notch depth and pitch and based on the assumption that periodic roughness notches are equivalent to periodic cracks. In particular, $\sqrt{area}_R$ is given by:

$$\frac{\sqrt{area}_R}{2a_2} \simeq 2.97\left(\frac{a_1}{2a_2}\right) - 3.51\left(\frac{a_1}{2a_2}\right)^2 - 9.47\left(\frac{a_1}{2a_2}\right)^3 \qquad For \quad \frac{a_1}{2a_2} < 0.195 \tag{9}$$

$$\frac{\sqrt{area}_R}{2a_2} \simeq 0.38 \qquad For \quad 3 > \frac{a_1}{2a_2} > 0.195 \tag{10}$$

where a_1 is the roughness notch depth and $2a_2$ the pitch of adjacent roughness notches along the load axis. According to Murakami [12], the value of a_1 should coincide with the maximum value of roughness profile, so, for the case at hand, a_1 was assumed to be equal to $R_t = 9\mu m$, as determined by the previously described roughness measurements. The definition of $2a_2$ resulted to be a bit more complicated because the original model by Murakami considers a typical periodical roughness generated by traditional machining like, for example, turning. This is not the case, as shown in Fig. 14 (bottom), because the morphology of the surface finish is not periodical, but characterized by peculiar roughness pits more or less uniformly distributed on the surface.

The problem was faced measuring, by a software for image processing applied to the pictures of the surfaces of four different wires taken by the aforementioned optical microscope, the distance (pitch) between the centres of sequences of roughness pits, aligned along the load axis, and applying a statistical analysis. Such an analysis provided a mean pitch equal to $300\mu m$ with a standard deviation equal to $35\mu m$, so $2b$ was assumed to be equal to $300\mu m$. The ratio $\frac{a_1}{2a_2}$ resulted, then, equal to 0.03, imposing the use of Eq. 9, which provided a $\sqrt{area}_R$ value equal to $25.7\mu m$. Finally, such a $\sqrt{area}_R$ value, along with the $\mu \pm \sigma$ limits of the measured Vickers Hardness reported in Table 5, was inserted in Eq. 8 and provided the estimation of the transition stress level (shaded red region in Fig. 13). Since the region of the estimated transition stress level and the one of the experimentally derived one are very close and partially overlapping, it can be concluded that the bench is actually effective and truthful in carrying out fatigue tests on full-scale wires for spring manufacturing.

5 Conclusions

The paper has been devoted to the fatigue life characterization of steel wires for coil springs. The fatigue characterization of the full-scale wire is of crucial importance for the manufacturing of high performance springs. An innovative four-point bending test bench able to test the full-scale wires has been presented. The current experimental approach based on bending fatigue tests is justified since bending stresses represent an important factor in spring failures. Additionally torsion fatigue tests on wires seem, at the present, unfeasible.

The presented test bench by characterizing full-scale wires, enables for the full understanding of the failure mechanisms related to the actual surface finishing and subsurface inclusions. The effects on wire fatigue of manufacturing process parameters (drawing and/or tempering) can be analysed. Also, the bench can be placed at the end of a production line, for quality assessment.

The effectiveness and reliability of the bench was demonstrated through experimental tests on different sets of wires. Two identical sets of precise ground bars made of 39NiCrMo3 tempered steel were tested on two different prototypes of the test bench showing no statistical differences on the obtained fatigue data. Additionally, a comparison with data related to standard fatigue tests taken from the literature confirmed the consistency of the data.

A set of 14 specimens of a 11.5 mm 54Cr6 steel wire employed for spring manufacturing was tested up to 10^8 cycles, i.e. both in the HCF and VHCF regime. Tests were fully satisfactory, the failing section of the wire was found within the expected region and the analysis of the fracture surfaces revealed the typical features of the rotating bending loading scheme. Even in this case, the acquired data were significantly consistent with literature fatigue data obtained from mirror-polished specimens.

In the next future, the new bench will be used for VHCF testing. The bench is currently used for assessing the fatigue properties of wires as they result from manufacturing process. In particular, the effects of surface finishing on fatigue of wires are assessed on a daily industrial base.

Acknowledgements F.A.R. S.p.A. belonging to Steelgroup Holding, Italy is gratefully acknowledged. Mr. Fabio Pederiva and Mr. Luca Merlini have provided direct support during the whole project. A special thank to Dr. Mario Pennati, who designed the test bench. Mr. Dario Crema, Dr. Andrea Gianneo, Mr. Davide Pegoraro and Mr. Giacomo Sala have given substantial contribution.

The Italian Ministry of Education, University and Research is acknowledged for the support provided through the Project "Department of Excellence LIS4.0 - Lightweight and Smart Structures for Industry 4.0".

Compliance with Ethical Standards

Conflict of interest: This study was funded by F.A.R. S.p.A. belonging to Steelgroup Holding

References

1. Abe, T., Furuya, Y., Matsuoka, S.: Gigacycle fatigue properties of 1800 MPa class spring steels. Fatigue and Fracture of Engineering Materials and Structures **27**(2), 159–167 (2004). DOI 10.1111/j.1460-2695.2004.00737.x
2. Grad, P., Reuscher, B., Brodyanski, A., Kopnarski, M., Kerscher, E.: Mechanism of fatigue crack initiation and propagation in the very high cycle fatigue regime of high-strength steels. Scripta Materialia **67**(10), 838–841 (2012). DOI 10.1016/j.scriptamat.2012.07.049
3. Kaiser, B., Pyttel, B., Berger, C.: VHCF-behavior of helical compression springs made of different materials. International Journal of Fatigue **33**(1), 23–32 (2011). DOI 10.1016/J.IJFATIGUE.2010.04.009
4. Pyttel, B., Brunner, I., Kaiser, B., Berger, C., Mahendran, M.: Fatigue behaviour of helical compression springs at a very high number of cycles –

Investigation of various influences. International Journal of Fatigue **60**, 101–109 (2014). DOI 10.1016/J.IJFATIGUE.2013.01.003
5. Zoroufi, M., Fatemi, A.: A Guideline for Fatigue Testing of Components. In: E.E. Gdoutos (ed.) Experimental Analysis of Nano and Engineering Materials and Structures, pp. 173–174. Springer Netherlands, Dordrecht (2007)
6. Bacher-Hoechst, M., Issler, S.: Assessment of Very High Cycle Fatigue (VHCF) Effects in Practical Applications. Procedia Engineering **66**, 26–33 (2013). DOI https://doi.org/10.1016/j.proeng.2013.12.059
7. Godfrey, H.J.: The fatigue and bending properties of cold drawn steel wire. Trans. Amer. Soc. Metals **29**(52), 133–168 (1941)
8. Shelton, S., Swanger, W.: Fatigue properties of steel wire. Journal of Research of the National Bureau of Standards **14**(1), 17–32 (1935). DOI 10.6028/jres.014.005
9. Zhang, J., Yang, Z., Li, S., Hui, W., Weng, Y.: Ultra high cycle fatigue behavior of automotive high strength spring steels 54SiCrV6 and 54SiCr6. Acta Metallurgica Sinica **42**, 259–264 (2006)
10. Berto, F., Lazzarin, P., Yates, J.R.: Multiaxial fatigue of V-notched steel specimens: A non-conventional application of the local energy method. Fatigue and Fracture of Engineering Materials and Structures **34**(11), 921–943 (2011). DOI 10.1111/j.1460-2695.2011.01585.x
11. Akiniwa, Y., Stanzl-Tschegg, S., Mayer, H., Wakita, M., Tanaka, K.: Fatigue strength of spring steel under axial and torsional loading in the very high cycle regime. International Journal of Fatigue **30**(12), 2057–2063 (2008). DOI 10.1016/J.IJFATIGUE.2008.07.004
12. Murakami, Y.: Metal Fatigue: Effects of Small Defects and Nonmetallic Inclusions. Elsevier, Oxford, UK (2002)
13. Pöllänen, I., Martikka, H.: Optimal re-design of helical springs using fuzzy design and FEM. Advances in Engineering Software **41**(3), 410–414 (2010). DOI 10.1016/J.ADVENGSOFT.2009.03.010
14. Zhu, Y., Wang, Y., Huang, Y.: Failure analysis of a helical compression spring for a heavy vehicle's suspension system. Case Studies in Engineering Failure Analysis **2**(2), 169–173 (2014). DOI 10.1016/J.CSEFA.2014.08.001
15. Niemann, G., Winter, H., Höhn, B.R.: Maschienenelemente. Springer-Verlag, Berlin (2005)
16. Hartmann, E., Howell, F.: Laboratory Fatigue Testing of Materials. In: G. Sines, J.L. Waisman (eds.) Metal fatigue. McGraw-Hill Co., New York (1959)
17. Nakamura, H., Nishihara, T.: New Fatigue Testing Machine for Wire Rod (in Japanese). Utility Model Publication **45**, 45–49 (1959)
18. Huck, M.: Rotating bending testing machine for long round rods. Patent WO/1995/002810 (1995)
19. IABG: Rotating bending test machine (RBTM)
20. Ballo, F., Carboni, M., Mastinu, G., Previati, G.: Tempered Wire Fatigue Testing. In: SAE Technical Paper 2019-01-0532, pp. 1–5 (2019). DOI 10.4271/2019-01-0532.Abstract
21. Budynas, R.G., Nisbett, J.K.: Shigley's Mechanical Engineering Design. McGraw Hill (2014)
22. Campagnolo, A., Dabalà, M., Meneghetti, G.: Effect of Salt Bath Nitrocarburizing and Post-Oxidation on Static and Fatigue Behaviours of a Construction Steel. Metals **9**(12), 1–19 (2019). URL www.mdpi.com/journal/metals
23. Baragetti, S., Tordini, F.: Fatigue resistance of PECVD coated steel alloy. International Journal of Fatigue **29**(9-11), 1832–1838 (2007). DOI 10.1016/J.IJFATIGUE.2007.02.008
24. EN10083-3:2006: Steels for quenching and tempering — Part 3: Technical delivery conditions for alloy steels. Standard, European Standard (2006)
25. ASTM-E739: Standard Practice for Statistical Analysis of Linear or Linearized Stress-Life and Strain-Life Fatigue Data. Standard, ASTM International (2010)
26. EN10270-2:2011: Oil hardened and tempered spring steel wire. Standard, European Standard (2011)
27. ASTM-E8/E8M-16ae1: Standard Test Methods for Tension Testing of Metallic Materials. Standard, ASTM International (2016)
28. ASTM-E140-12B(2019)e1: Standard Hardness Conversion Tables for Metals Relationship Among Brinell Hardness, Vickers Hardness, Rockwell Hardness, Superficial Hardness, Knoop Hardness, Scleroscope Hardness, and Leeb Hardness. Standard, ASTM International (2019)
29. ISO6508-1:2016: Metallic materials — Rockwell hardness test — Part 1: Test method. Standard, International Organization for Standardization (2016)